A Multiconductor Model for Finite-Element Eddy-Current Simulation

Herbert De Gersem and Kay Hameyer

***Abstract*—The stranded-conductor finite-element model does not account for the skin and proximity effects in a multiconductor system. The solid conductor model considers the true geometry, all the individual conductors, and their connections but may lead to unmanageably huge models. The multiconductor model proposed here, does not necessarily consider all geometrical details but instead, discretizes the inner geometry and voltage drop and enforces the typical current redistribution in multiconductor configurations in a weak sense. The magnetic and electric meshes are independently and adaptively refined which results in an optimal error control and accurate results for relatively small models.**

***Index Terms*—Circuit simulation, eddy currents, finite element methods, windings.**

I. Introduction

MULTICONDUCTOR windings are sets of conductors, electrically insulated from each other and connected in series or parallel. The individual conductors experience skin and proximity effects, characterized by the *skin depth*

$$\delta = \sqrt{\frac{1}{f\pi\mu\sigma}} \tag{1}$$

where f is the frequency, μ is the permeability, and σ is the conductivity. The skin depth may be different in the x and y direction due to anisotropic permeabilities. The characteristic extents of a single wire in the multiconductor system with respect to the main axes are denoted by d_x and d_y. If $d_x \ll \delta$ and $d_y \ll \delta$, the stranded-conductor model is appropriate [1]. If $d_x \gg \delta$ and $d_y \gg \delta$, impedance boundary conditions are commonly applied [2]. If d_x, d_y, and δ are of the same order of magnitude, the skin effect is resolved by eddy-current simulation using the solid conductor model. The unidirectional skin effect as observed in foil conductors, i.e., $d_x \ll \delta$ and d_y of the same order of magnitude as δ, is considered in [3] and [4]. These four modeling approaches are limiting cases for particular kinds of current redistribution (Fig. 1). In many models, the influence of the skin effect on the global behavior of the model is not negligible although its local influence does not have to be computed in detail.

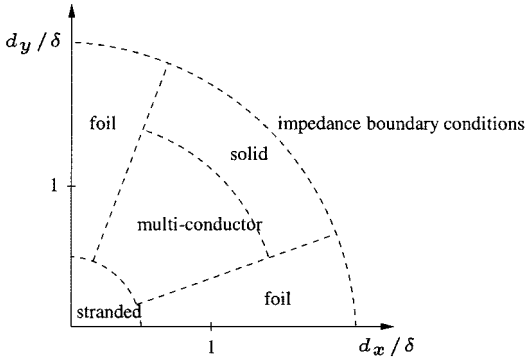

Fig. 1. Application range of the solid, stranded, foil, and multiconductor models and impedance boundary conditions.

Multiconductor systems arise in almost all electrical energy transducers. The devices may feature a large number of multiconductor systems, each consisting of a considerable number of turns. This may hamper the simulation of the overall device. Several model reduction techniques for multiconductor systems exist, e.g., analytical macroelements [5], inner node elimination [6] and parameter extraction [7]. They constitute an *a priori* model reduction, which may hinder adaptive error control during numerical simulation. In this paper, it is suggested to approximate the troublesome geometries by an additional discretization for the voltage and to incorporate this in the magnetic finite-element (FE) model. An error estimator adaptively refines the multiconductor model during the simulation.

II. Magnetodynamic Model

For convenience, a two-dimensional time-harmonic formulation is considered. The derivation of a multiconductor model for three-dimensional FE models, transient formulations, or anisotropic materials is similar. The magnetodynamic formulation is

$$-\frac{\partial}{\partial x}\left(\frac{1}{\mu}\frac{\partial \underline{A}_z}{\partial x}\right) - \frac{\partial}{\partial y}\left(\frac{1}{\mu}\frac{\partial \underline{A}_z}{\partial y}\right) + \jmath\omega\sigma\underline{A}_z = \frac{\sigma}{\ell_z}\Delta\underline{V} \tag{2}$$

with ω the pulsation, ℓ_z the length of the model, $\underline{A}_z$ the phasor of the z component of the magnetic vector potential and $\Delta\underline{V}$ the phasor of the voltage drop between front and rear ends of the model. The partial differential equation is discretized on the

Manuscript received July 5, 2001. This work was supported in part by the Belgian "Fonds voor Wetenschappelijk Onderzoek Vlaanderen" under Grant G.0427.98 and in part by the Belgian Ministry of Scientific Research under Grant IUAP no. P4/20.

H. De Gersem was with the Katholieke Universiteit Leuven, Department ESAT, Division ELEN. He is now with the FB 18 Elektrotechnik und Informationstechnik, Fachgebiet Theorie Elektromagnetischer Felder, Technische Universität Darmstadt, D-64289 Darmstadt, Germany (e-mail: degersem@temf.de).

K. Hameyer is with the Katholieke Universiteit Leuven, Department ESAT, Division ELEN, B-3001 Leuven-Heverlee, Belgium (e-mail: kay.hameyer@esat.kuleuven.ac.be).

Publisher Item Identifier S 0018-9464(02)02348-8.

device cross section Ω by n_{fe} linear, triangular FEs $N_i(x, y)$, yielding the system of equations

$$K\underline{u} - \underline{f} = 0 \tag{3}$$

$$K_{ij} = \int_\Omega \left(\frac{1}{\mu} \nabla N_i \cdot \nabla N_j + \jmath\omega\sigma N_i N_j \right) \mathrm{d}\Omega \tag{4}$$

$$\underline{f}_i = \int_\Omega \frac{\sigma}{\ell_z} \Delta\underline{V} N_i \, \mathrm{d}\Omega \tag{5}$$

and $\underline{u}_j$ the degrees of freedom (DOFs) for $\underline{A}_z$.

III. Modeling Assumptions

Consider a multiconductor with cross section $\Omega_{\mathrm{mc}} \subset \Omega$, consisting of N_{mc} conductors with cross sections Ω_m, $m = 1, \ldots, N_{\mathrm{mc}}$ and connected in series. The cross sections Ω_m may have different shapes but have the same area S_m. The cross-sectional area of Ω_{mc} is S_{mc}. The union of all conductor cross sections, $\Omega_{\mathrm{cond}} = \bigcup_{m=1}^{N_{\mathrm{mc}}} \Omega_m$, is contained in Ω_{mc} but may be smaller than Ω_{mc}. The difference $\Omega_{\mathrm{mc}} \backslash \Omega_{\mathrm{cond}}$ is occupied by insulation material, cooling ducts, and gaps which are supposed to be uniformly distributed over Ω_{mc} and to have a homogeneous permeability μ_{gap} and a zero conductivity. The voltage drop is aligned with the z direction, is constant over each Ω_m and is zero in $\Omega_{\mathrm{mc}} \backslash \Omega_{\mathrm{cond}}$

$$\Delta\underline{V}(x, y) = \begin{cases} \Delta\underline{V}_m, & \text{in } \Omega_m,\ m = 1, \ldots, N_{\mathrm{mc}} \\ 0, & \text{in } \Omega_{\mathrm{mc}} \backslash \Omega_{\mathrm{cond}}. \end{cases} \tag{6}$$

The voltage drop differs from one conductor to the other due to the vicinity of ferromagnetic cores and because of inhomogeneous conductivities, e.g., due to local heating.

IV. Continuous Multiconductor Model

The true multiconductor model obeys (2) and an integral constraint over each Ω_m, $m = 1, \ldots, N_{\mathrm{mc}}$

$$\int_{\Omega_m} \left(\frac{\sigma}{\ell_z} \Delta\underline{V}_m - \jmath\omega\sigma \underline{A}_z(x, y) \right) \mathrm{d}\Omega = \underline{I}_{\mathrm{mc}}. \tag{7}$$

The voltage drop across the multiconductor is

$$\Delta\underline{V}_{\mathrm{mc}} = \sum_{m=1}^{N_{\mathrm{mc}}} \Delta\underline{V}_m. \tag{8}$$

Consider now the limiting case in which N_{mc} tends to infinity and, hence, S_m becomes very small. Still, suppose all conductors to have the same cross-section area and the conductive and nonconductive parts of Ω_{mc} to be uniformly mixed. The insulation material is not explicitly considered in the model. The material parameters in the magnetic equations (2), (4), and (5) are replaced by the homogenized parameters

$$\tilde{\sigma}(x, y) = f_{\mathrm{mc}} \sigma(x, y) \tag{9}$$

$$\tilde{\mu}(x, y) = f_{\mathrm{mc}} \mu(x, y) + (1 - f_{\mathrm{mc}}) \mu_{\mathrm{gap}} \tag{10}$$

with the *fill factor*

$$f_{\mathrm{mc}} = \frac{N_{\mathrm{mc}} S_m}{S_{\mathrm{mc}}} \tag{11}$$

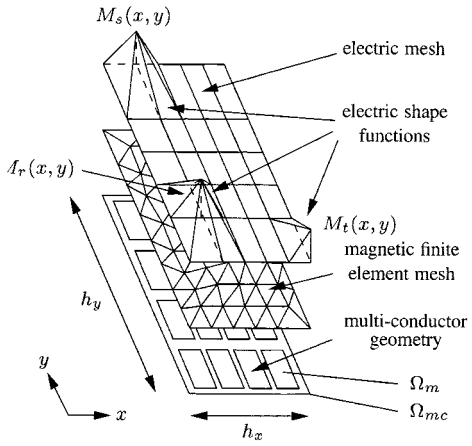

Fig. 2. Cross section of the multiconductor, the magnetic mesh, the electric mesh, and three electric shape functions.

accounting for the nonconductive regions included in Ω_{mc}. The true constraints (7) tend to the continuous constraint

$$\frac{\tilde{\sigma}}{\ell_z} \Delta\underline{V}(x, y) - \jmath\omega\tilde{\sigma} \underline{A}_z(x, y) = \underline{J}_{\mathrm{mc}} = \frac{f_{\mathrm{mc}}}{S_m} \underline{I}_{\mathrm{mc}} \quad \text{in } \Omega_{\mathrm{mc}}. \tag{12}$$

The voltage across the overall multiconductor is obtained by averaging $\Delta\underline{V}(x, y)$ over Ω_{mc} and multiplying by N_{mc}

$$\Delta\underline{V}_{\mathrm{mc}} = \frac{N_{\mathrm{mc}}}{S_{\mathrm{mc}}} \int_{\Omega_{\mathrm{mc}}} \Delta\underline{V}(x, y) \, \mathrm{d}\Omega. \tag{13}$$

It may be beneficial to model a multiconductor system with a considerable number of turns by the continuous model (12) and (13) rather than the true relations (7) and (8) which require the geometry of each individual conductor to be considered.

V. Discrete Multiconductor Model

To discretize the continuous multiconductor model, an additional mesh for the voltage drop is constructed (Fig. 2). To simplify the implementation, a tensor grid is preferred. $\Delta\underline{V}(x, y)$ is resolved by n_{mc} *electric shape functions* $M_q(x, y)$

$$\Delta\underline{V}(x, y) = \sum_{q=1}^{n_{\mathrm{mc}}} \Delta\underline{V}_q M_q(x, y) \tag{14}$$

with $\Delta\underline{V}_q$ the associated DOFs. Equation (5) becomes

$$\underline{f}_i = \sum_{q=1}^{n_{\mathrm{mc}}} \Delta\underline{V}_q \underbrace{\int_{\Omega_{\mathrm{mc}}} \frac{\tilde{\sigma}}{\ell_z} N_i M_q \, \mathrm{d}\Omega}_{z_{iq}}. \tag{15}$$

A weak formulation of the multiconductor model is obtained by weighting (12) by the electric shape functions $M_p(x, y)$

$$\sum_{q=1}^{n_{\mathrm{mc}}} \Delta\underline{V}_q \overbrace{\int_{\Omega_{\mathrm{mc}}} \frac{\tilde{\sigma}}{\ell_z} M_p M_q \, \mathrm{d}\Omega}^{g_{pq}} - \sum_{j=1}^{n_{fe}} \underline{u}_j \overbrace{\int_{\Omega_{\mathrm{mc}}} \jmath\omega\tilde{\sigma} M_p N_j \, \mathrm{d}\Omega}^{\jmath\omega\ell_z z_{pj}} - \underbrace{\int_{\Omega_{\mathrm{mc}}} \frac{f_{\mathrm{mc}}}{S_m} M_p \, \mathrm{d}\Omega}_{s_p} \underline{I}_{\mathrm{mc}} = 0. \tag{16}$$

The voltage across the overall multiconductor is

$$\Delta \underline{V}_{\mathrm{mc}} = \sum_{q=1}^{n_{\mathrm{mc}}} \Delta \underline{V}_q \underbrace{\frac{N_{\mathrm{mc}}}{S_{\mathrm{mc}}} \int_{\Omega_{\mathrm{mc}}} M_q \, \mathrm{d}\Omega}_{s_q}. \tag{17}$$

The weak formulation of the magnetodynamic problem (3), the weak formulation of the current constraints (16), and the integration of the discrete voltage drop (17) are assembled into the coupled system of equations

$$\begin{bmatrix} K_{ij} & -z_{iq} & 0 \\ -z_{pj} & \chi g_{pq} & -\chi s_p \\ 0 & -\chi s_q & 0 \end{bmatrix} \begin{bmatrix} \underline{u}_j \\ \Delta \underline{V}_q \\ \underline{I}_{\mathrm{mc}} \end{bmatrix} = \begin{bmatrix} 0 \\ 0 \\ -\chi \Delta \underline{V}_{\mathrm{mc}} \end{bmatrix} \tag{18}$$

with $\chi = 1/\jmath\omega\ell_z$ a factor symmetrizing the system. The system has the nature of a mixed formulation [8]. Because the coefficients K_{ij} and χg_{pq} scale differently, it is recommended to apply an explicit diagonal scaling of (18) before solving. The system is solved by a Quasi-Minimal Residual method adapted to complex symmetric systems [9], preconditioned by successive over relaxation.

The multiconductor model can be coupled to a circuit model accounting for active and passive components outside the finite-element model. The treatment of arbitrary circuit connections follows the topological approach presented in [10].

VI. Adaptive Mesh Refinement

The electric mesh does not coincide with the magnetic mesh nor with the true multiconductor geometry. Therefore, adaptive mesh refinement can be applied independently. The possibility of independent error control is one of the most attractive features of the multiconductor model. The magnetic mesh is refined based on indications of large eddy currents and large ferromagnetic saturation. The error indicator for the electric mesh detects large variations of the voltage drop.

To preserve the consistency of the multiconductor model, the discrete weak formulation (16) has to converge towards the true model (7) rather than towards the continuous representation (12). As a consequence, the supports of the electric shape functions have to converge towards the single-conductor cross sections. This is different from a conventional discretization where convergence corresponds to a vanishing mesh size. The consistency of the electric discretization of the multiconductor model is guaranteed by the following procedure. At places where refinement would bring up electric elements smaller than the extent of a single conductor, the true geometry is restored (Fig. 3). The discrete formulation (16) implicitly incorporates the true model (7) if a single, constant shape function is assigned to each conductor that shows up in Ω_{mc} because of refinement. The parts of the insulation that are restored by the refinement procedure, are expelled from the electric mesh. As a consequence, the electric mesh may become disconnected and the fill factor has to be adapted accordingly. The limiting case when the voltage drop is discretized by N_{mc} constant electric shape functions defined at Ω_m, $m = 1, \ldots, N_{\mathrm{mc}}$, and the fill factor is one, corresponds to the explicit modeling of each of the individual conductors as a solid conductor, and, hence, constitutes the true multiconductor model (7) and (8). For technical models, however, a sufficient accuracy is already achieved when the electric mesh is much coarser than the true geometry. If local effects would become important, the error indicator will detect them and invoke substantial refinement at those places, probably leading to a local recovery of the true geometry of the multiconductor system.

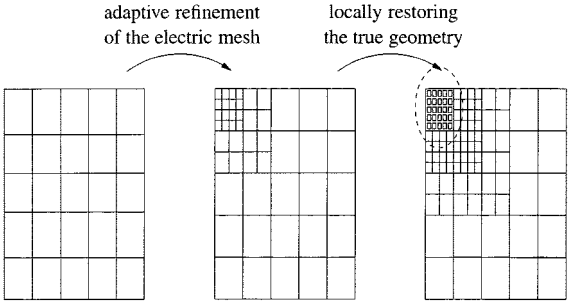

Fig.3. Consistent adaptive refinement of the electric tensor grid when the error estimator indicates large variations of the voltage drop at the left upper corner of the multiconductor cross section (at a certain point, further refinement corresponds to restoring the original geometry).

VII. Nonmatching Integrations

The efficiency of the multiconductor model is strongly related to the flexibility of selecting and refining the meshes. It is recommended to allow an independent construction and refinement of both meshes. Hence, the supports of $N_i(x, y)$ and $M_q(x, y)$, in general, do not match. This considerably hinders the evaluation of the hybrid integrals in z_{iq}. A numerical integration scheme, e.g., Gaussian quadrature, encounters problems to select appropriate integration points or may require a huge number of points in order to sample both meshes at a sufficient rate. Here, a semi-analytical technique is favored. A composite mesh is built by gathering all vertices and edges of both the magnetic and the electric mesh. The intersections of the edges of the different meshes with respect to each other have to be computed with a sufficient accuracy, preferably using exact arithmetic. Both $N_i(x, y)$ and $M_q(x, y)$ can be exactly represented on the composite mesh on which the multiplications and integrations can then be performed exactly. The required computation time is substantial but is still acceptable when compared with the overall computation time. To avoid hybrid integrals, one could use the composite mesh for both electric and magnetic discretization. This approach, however, does not pay off because the substantially larger system of equation would eliminate the efficiency of the multiconductor model.

VIII. Convergence of the Multiconductor Discretization

The convergence of the mixed discretization technique is studied for a model problem. The multiconductor contains 250 conductors. All feature the same conductivity and permeability. The conductors are electrically insulated from each other, are connected in series, and carry an alternating current. No flux leaves the model. Within each conductor, the magnetic field is expressed by the analytical solution of (2) for a rectangular domain. The analytical solution for the multiconductor system is derived by applying the interface conditions at the borders of the conductors and requiring the current to be the same in

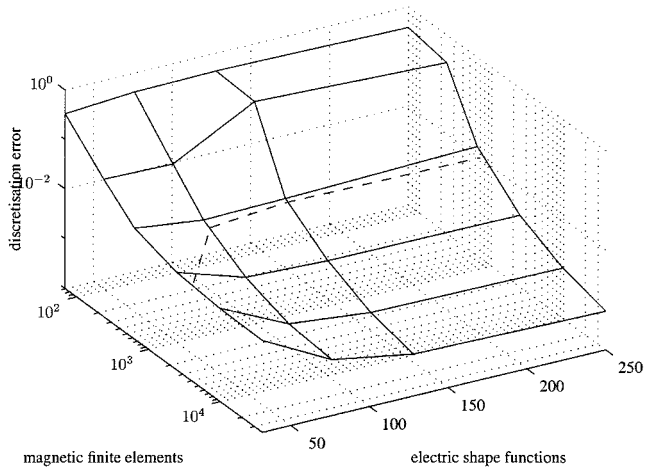

Fig. 4. Convergence of the discretization error of the magnetic vector potential field of the multiconductor model (the dashed line is a line of constant error).

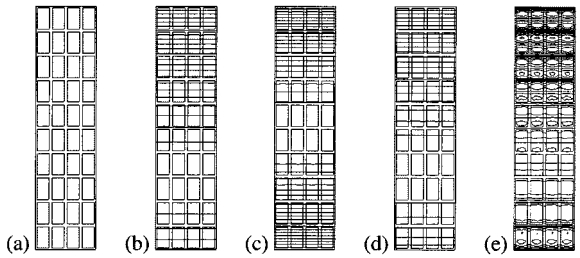

Fig. 5. (a) Geometry, (b) real, and (c) imaginary components of the magnetic flux in a single-layer stator slot at 50 Hz. (d) Real and (e) imaginary components of the magnetic flux in the multiconductor model at 500 Hz.

each conductor. The discretization error of the magnetic vector potential field obtained by the proposed multiconductor model, is measured in the L2-norm with respect to the analytical solution (Fig. 4). The error decays when the magnetic and/or electric meshes are refined. The dashed line denotes loci for which the error is identical. The experiment indicates that the discretization error depends more on the discretization of the magnetic field than on the discretization of the electric voltage drop. As a consequence, it is sometimes more advantageous to apply a finer magnetic mesh than to consider all geometrical details of the multiconductor system.

IX. Example: Machine Windings

The multiconductor model is applied to simulate the harmonic losses in induction machine windings [11] (Fig. 5). Since these devices are supplied by variable frequency, the relative importance of the higher harmonic distortion increases and the additional joule losses are not negligible. These effects are commonly taken into account in analytical models by the frequency-dependent eddy-current factor which can be provided by a FE model of a single stator slot [12]. A leakage flux impinging on the conductor is applied to the model by a difference in magnetic vector potential between the top and the bottom of the slot. A conventional model considers the true geometry consisting of the conductors, the insulation, and the cooling ducts. It treats the coil as a series connection of a number of solid conductors, each with their own unknown voltage. For many cases, the multiconductor model offers a sufficient accuracy while avoiding an excessive amount of mesh nodes and voltage unknowns. At 50 Hz, no significant skin effect is observed. At 500 Hz, substantial losses are introduced. The multiconductor model equipped with independent mesh refinement and external circuit coupling, enables the simulation of the model for all possible frequencies by the same conductor model (Fig. 6).

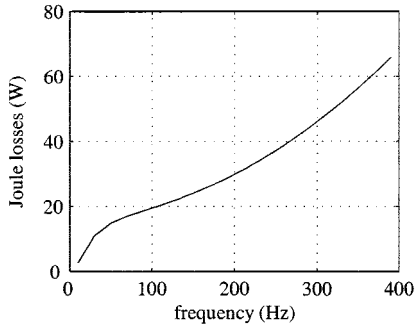

Fig. 6. Harmonic losses in a stator winding of an induction machine.

X. Conclusion

The multiconductor model developed here, enables the simulation of complicated coil configurations with relatively small models by using an additional discretization for the conductor's voltage drop. It offers more modeling flexibility when compared with the solid and stranded-conductor models. The automated error control and independent mesh refinement yields small models while guaranteeing the prescribed accuracy.

References

[1] G. Bedrosian, "A new method for coupling finite-element field solutions with external circuits and kinematics," *IEEE Trans. Magn.*, vol. 29, pp. 1664–1668, Mar. 1993.

[2] A. M. El-Sawy Mohamed, "Finite-element variational formulation of the impedance boundary condition for solving eddy current problems," *Inst. Elect. Eng. Proceedings Science, Measurement and Technology*, vol. 142, no. 4, pp. 293–298, July 1995.

[3] H. De Gersem and K. Hameyer, "A finite-element model for foil winding simulation," *IEEE Trans. Magn.*, vol. 37, pp. 3427–3432, Sept. 2001.

[4] P. Dular and C. Geuzaine, "A magnetic field magnetodynamic finite-element formulation for foil winding inductors," *IEEE Trans. Magn.*, submitted for publication.

[5] A. Kladas and A. Razek, "Numerical calculation of eddy-currents and losses in squirrel cage induction motors due to supply harmonics," in *Proc. Int. Conf.Electrical Machines (ICEM88)*, vol. 2, Pisa, Italy, Sept., pp. 65–69.

[6] Á. Szűcs and A. Arkkio, "Consideration of eddy currents in multiconductor windings using the finite element method and the elimination of inner nodes," *IEEE Trans. Magn.*, vol. 35, pp. 1147–1150, May 1999.

[7] I. Munteanu, T. Wittig, T. Weiland, and D. Ioan, "FIT/PVL circuit-parameter extraction for general electromagnetic devices," *IEEE Trans. Magn.*, vol. 36, pp. 1421–1425, July 2000.

[8] F. Brezzi and M. Fortin, *Mixed and Hybrid Finite Element Methods*. Berlin, Germany: Springer-Verlag, 1991.

[9] R. W. Freund, "Conjugate gradient-type methods for linear systems with complex symmetric coefficient matrices," *SIAM J. Scientific Computing*, vol. 13, pp. 425–448, Jan. 1992.

[10] H. De Gersem, R. Mertens, U. Pahner, R. Belmans, and K. Hameyer, "A topological method used for field-circuit coupling," *IEEE Trans. Magn.*, vol. 34, pp. 3190–3193, Sept. 1998.

[11] S. J. Salon, L. Ovacik, and J. F. Balley, "Finite-element calculation of harmonic losses in AC machine windings," *IEEE Trans. Magn.*, vol. 29, pp. 1442–1445, Mar. 1993.

[12] R. Richter, "Die Induktionsmaschinen," in *Elektrische Maschinen*, 2nd ed. Basel, Switzerland: Birkhauser, 1963, vol. 4.